Metal Discovery by Highly Sensitive Microwave Multi-Band Metamaterial-Inspired Sensors

Ghaleb Al-Duhni and Nantakan Wongkasem*

Abstract—A simple, compact, contactless, and high sensitivity metamaterial-inspired sensor has been developed to detect and classify precious transition metals in the S- and C-band regime, using reflection coefficients. A multi-band metamaterial, quadruple concentric circular split ring resonator, is specifically designed as a sensing enhancer, where the additional bands can effectively trigger the electromagnetic properties, as well as enhance the differentiation between the testing metal samples. The proposed sensor was tested on precious transition metals, silver, platinum, and gold thin slabs of various thicknesses, from $0.5\,\mu m$ to $3\,mm$. Five resonances were established in the frequency range of 2–8 GHz. Distinguishable frequency responses generated from different metal samples at those five resonances specify the capability of classifying the metal contents and thicknesses.

1. INTRODUCTION

Most existing metal sensors are based on the chemical and optical properties of metal substances [1–12], concentrating on the reaction between the substance atoms and catalysts [1, 3, 7], or light excitation [8–12]. Electroreduction from acids ($AuCl_4$ and $[PdCl_4]_2$) was used for recovering gold (Au) and palladium (Pd) [1]. Silver (Ag) and Au were detected using PH-sensitivity [2] and aminoantipyrine solid [3] by X-ray fluorescent system [7]. Surface plasmon, the collective charge oscillations, that occur at the interface between conductors and environment, are mainly used in optical metal sensors. An optical fiber sensor based on surface plasmon resonance for Ag in water contamination generated two resonances between 400 and 500 THz, for thickness of 2540 nm [8]. A quartz crystal microbalance was tested for gold ions with thickness varying from 0 to $100\,\mu m$, where a resonance near 650 nm was found [9]. Fluorescence absorption technique was implemented to improve sensor sensitivity for Au nanoparticle detection [10]. The thickness of Au in the range of 8–60 nm was calculated by its plasmonic behavior in the visible to infrared regime, from 640 to 950 nm [11]. One resonance was found in between 1200 nm–1350 nm, while the Ag thickness of the 3–20 nm range is calculated [12].

Currently there are several commercial metal detectors [13–19], mostly operating in low radio frequency (RF) ranges, 5.5 kHz–800 kHz [14]. These metal detectors based on eddy current-induced coil [19] typically consist of two loops, i.e., a transmitting loop to generate an eddy current and a receiving loop to detect the magnetic field of the eddy current [13]. The swept-frequency excitation method was introduced to improve the sensitivity to detect the eddy current within a wide range of frequencies [15]. Several RF frequency metal detectors are also used to detect unnecessary metals in food industry [13, 16]; however, they do not classify metal types. An approach based on the air-coil inductance change was implemented to detect ferrite existence in copper (Cu), iron (Fe), and aluminum (Al) [17, 18], by comparing the amplitude and phase angle of the received signal.

It is challenging to create an alternative and simple microwave sensor [20–25], a label-free, non-destructive, no-contact, instant measurement, low-cost, and low-profile sensor to identify the metals based on their electromagnetic (EM) properties, e.g., electric conductivity and permittivity in the microwave frequency regime. EM waves are mostly reflected from the medium with negative permittivity, a general behavior found in metals in microwave frequency. The waves can also penetrate the medium and pass through based on the medium skin depth or penetration depth: $\delta = \frac{1}{\sqrt{\pi f \mu \sigma}}$, where μ and σ are the medium permeability and conductivity, respectively, and f is the operating frequency. At δ, the wave amplitude is attenuated by the factor e^{-1}, or about 37% of its original peak. The skin depth is inversely proportional to the operating frequency; for example, the skin depths of Ag and Au are $1.002\,\mu m$ and $1.191\,\mu m$ at $4\,GHz$, and $31.7\,nm$ and $37.7\,nm$ at $4\,THz$. The attenuation (α) and phase (β) constant of good conductors are identical: $\alpha \approx \beta \approx \sqrt{\pi f \mu \sigma}$. Both constants depend directly on the operating frequency, permeability, and conductivity. The attenuation indicates the strength of the outgoing wave and how much the waves decay while they are propagating through the medium. It means that the transmission, reflection, and absorption from different metals of different thicknesses at different frequencies are unique.

In this research, we design a microwave sensor operating in the S- (2–4 GHz) and C- (4–8 GHz) bands to discover precious transition metals, focusing on the 3 best known precious metals: silver, platinum, and gold, of various thicknesses from $0.5\,\mu m$ to $3\,mm$. An S- and C- multi-band bowtie antenna was used as a transmitting port, where the reflection coefficients (S_{11}) were collected to analyze the material types and thicknesses. In the next section, the standalone bowtie antenna was first tested with various dielectric slabs ($\varepsilon_r = 1.5 - 10$) of $0.5\,\mu m$–$1\,mm$ thickness. The reflection responses showed a clear distinction among the slabs of different contents and thicknesses. The aforementioned standalone bowtie can also differentiate transition metals and metalloids, but it is challenging to classify the metal types. In response to this issue, a novel metamaterial (MTM) structure, a quadruple concentric circular split ring resonator (SRR), was designed to add to the bowtie antenna, as presented in Section 3. An array of three MTM structures are placed in between the bowtie antenna and the metal sample. The extra multi-resonances of MTMs are to improve the sensor's sensitivity. Five resonances were established in between the frequency of 2–8 GHz while the sensor was tested with thin Ag, Pt, and Au slabs. The reflection responses of Ag, Pt, and Au slabs can visibly separate the metal types and thicknesses.

2. S- AND C-BAND BOWTIE ANTENNAS AND ITS METAL, METALLOIS, AND DIELECTRIC DETECTING PROPERTIES

2.1. Multi S- and C-Band Bowtie Antenna

Although a simple quarter wavelength transmission line is commonly used in most MTM-inspired microwave sensors as a microwave transmission part, there was an attempt to implement a complementary SRR-loaded patch as an excitation port, where only reflection coefficients (S_{11}) were collected. In fact, a stand-alone antenna can be employed as a main sensing element [21, 22]. In this research, a bowtie antenna was chosen based on its structure and omnidirectional pattern. Not only can the radiation pattern and beamwidth of the bowtie antenna be easily designed to focus on the testing sample and the MTM enhancer, but also the operating frequency range can be controlled effectively. Therefore, more accurate data can be obtained, which is desirable for detecting different sample types. Its flat, printed structure helps to make the overall sensor size compact. A planar bowtie antenna was designed to operate in the S- and C-bands, where 3 of 5 bands are pronounced, at $4.17\,GHz$ ($-22.81\,dB$), $5.96\,GHz$ ($-12.74\,dB$), and $7.77\,GHz$ ($-10.10\,dB$). The bowtie was made of a two-sided 1 oz Cu FR-4 substrate with $\varepsilon_r = 4.4$. Figure 1 shows the bowtie dimensions, S_{11} parameter, and far-field radiation.

2.1.1. Bowtie Testing with Dielectric Slabs

The bowtie antenna was tested with a $100\,mm \times 60\,mm$ dielectric slab of 6 different thicknesses: $0.5\,\mu m$, $1\,\mu m$, $3\,\mu m$, $10\,\mu m$, $0.1\,mm$, and $1\,mm$. CST Microwave Studio [26] is implemented for the real-time simulations. The perfectly matched layer (PML) or open 'add space', a specific CST name, set for the system boundaries, ensures the least reflected and scattered waves from the boundaries. The estimated reflected level is 0.0001% or 0.01%. The sensitivity of the bowtie antenna was optimized by varying the
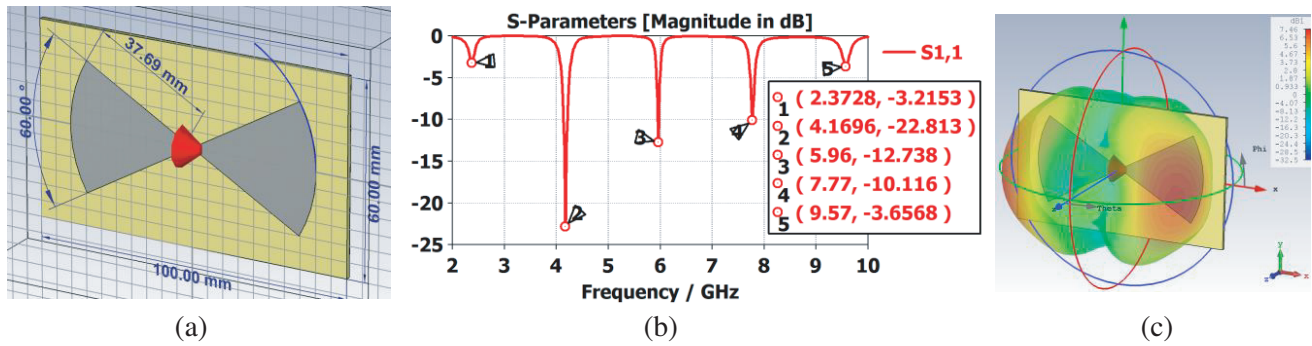
(a)   (b)   (c)

Figure 1. Bowtie dimensions, S_{11} parameter and far-field radiation.

spacing between the bowtie and the testing sample slab. The 18.75 mm showing the most pronounced detecting response was therefore selected in this study. The permittivity of the slab was varied (1.5, 2, 3, 5, and 10) to investigate the sensitivity of the antenna based on the reflection coefficients or S_{11}. While the dielectric slab is tested, all existing five S_{11} resonances were slightly shifted to a higher frequency, as shown in Figure 2. At least one of the five S_{11} resonances with a clear inclination can be used to identify the dielectric slab, i.e., 2nd, 3rd, and 4th for the 0.5 µm slabs; 1st, 2nd, 3rd, and 4th for the 1 µm slabs; 2nd, 3rd, 4th, and 5th for the 3 µm slabs; 4th and 5th for the 10 µm slabs; 5th for the 0.1 mm slabs; and 1st for the 1 mm slabs.

### 2.1.2. Bowtie Testing with Transition Metals and Metalloids

Metals or electropositive elements form positive ions by losing electrons during chemical reactions. They are characterized by bright luster and hardness. Metals grouped in the middle to the left-hand side of the periodic table consist of the alkali, alkaline earths, transition metals, post-transition, lanthanides, and actinides. Transition metals, where their valence electrons tend to fill the 'd' orbitals in their atoms, are located in the middle of the periodic table. They are known as good electrical conductors and have a high melting point [27]. Post-transition metals are located after transition metals and before metalloids in the periodic table. Their melting points are lower than the transition metals, same as their boiling points [28]. Aluminum is one of the most abundant elements on earth. Metalloid elements or semiconductors, i.e., boron (B), silicon (Si), germanium (Ge), arsenic (As), antimony (Sb), and tellurium (Te) [29], do not have too many free electrons comparative to conductors. They have common properties between metals and non-metals, so they behave like metals under certain conditions, and behave the same as non-metals under other conditions. Their electrons are more easily bound by atoms than conductors. The conductivity of metalloids is much lower than that of the transition metals and post-transition metals. Regarding thermal conductivity, precious transition metals have good thermal conductivity, but semiconductors such as silicon have better thermal conductivity than post-transition metals or even rich transition metals such as iron and manganese. The heat capacity of metalloids is better than that of transition metals and posttransition metals.

Here, several metals and metalloids were chosen to investigate the metal detecting and sensing properties of the bowtie antenna. We focus on their EM properties in the microwave frequency regime. Table 1 lists the electric conductivity of the precious transition metal: Ag, Pt, and Au, the abundant transition metals: Fe and Mn, the post transition or basic metals: Al and Sn, and metalloid: Si.

Figure 3 shows the reflection coefficient or S_{11} response of the bowtie testing with various thin metal and metalloid slabs (precious transition metals: gold (Au), silver (Ag), platinum (Pt); abundant transition metals: iron (Fe) and manganese (Mn); post transition or basic metals: aluminum (Al) and tin (Sn); metalloids: silicon (Si)) of 6 different thicknesses, i.e., 0.5 µm, 1 µm, 3 µm, 10 µm, 100 µm, and 1 mm.

All four resonances (4–4.4 GHz, 5.8–6.2 GHz, 7.5–8 GHz, and 9.4–9.8 GHz) of the metalloid, Si, and those of the metals (Au, Ag, Pt, Fe, Mn, Al, and Sn) stand out from those of the standalone bowtie antenna. Only the metals' 1st resonances are located at higher frequency, compared to that

of the bowtie's 1st resonance. All the rest (2nd, 3rd, and 4th) appear at lower frequency. However, these reflection responses of the transition and post transition metal slabs with the same thickness are marginally distinct. The detecting performance is not reaching its full potential. By carefully analyzing the reflection responses from the bowtie antenna, we can recognize different dielectrics, metalloids, and metals, but the metal types are not distinguishable.
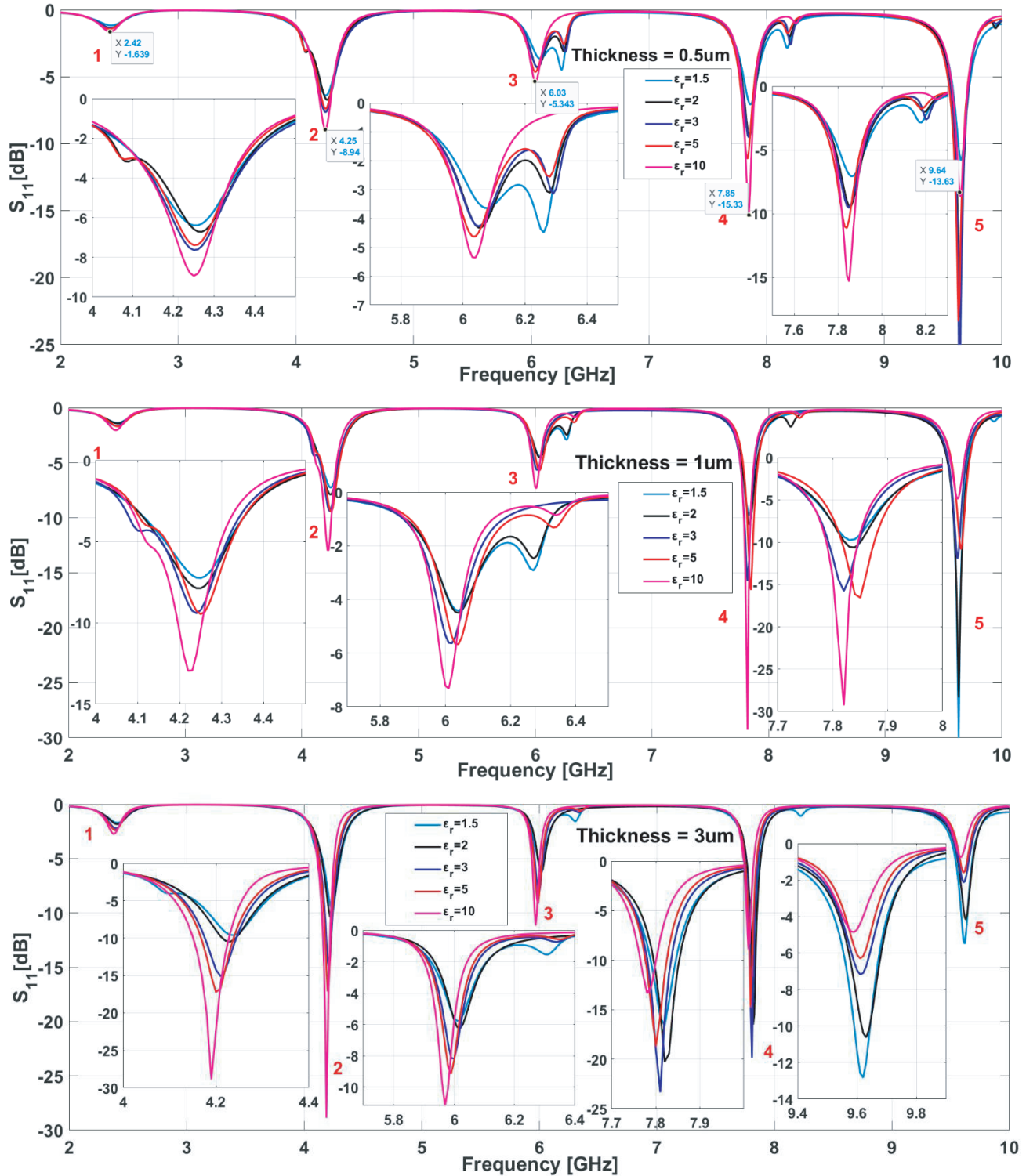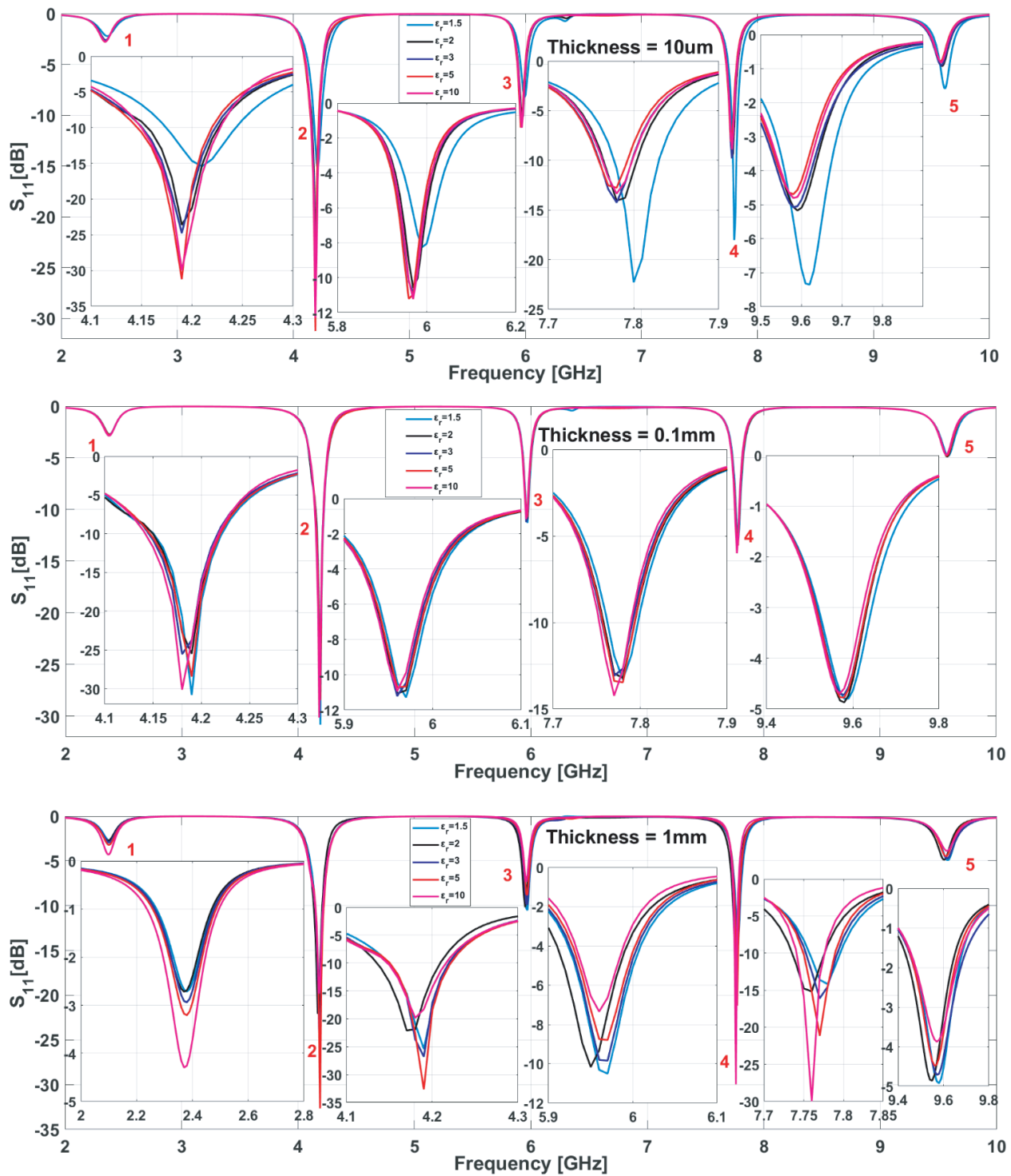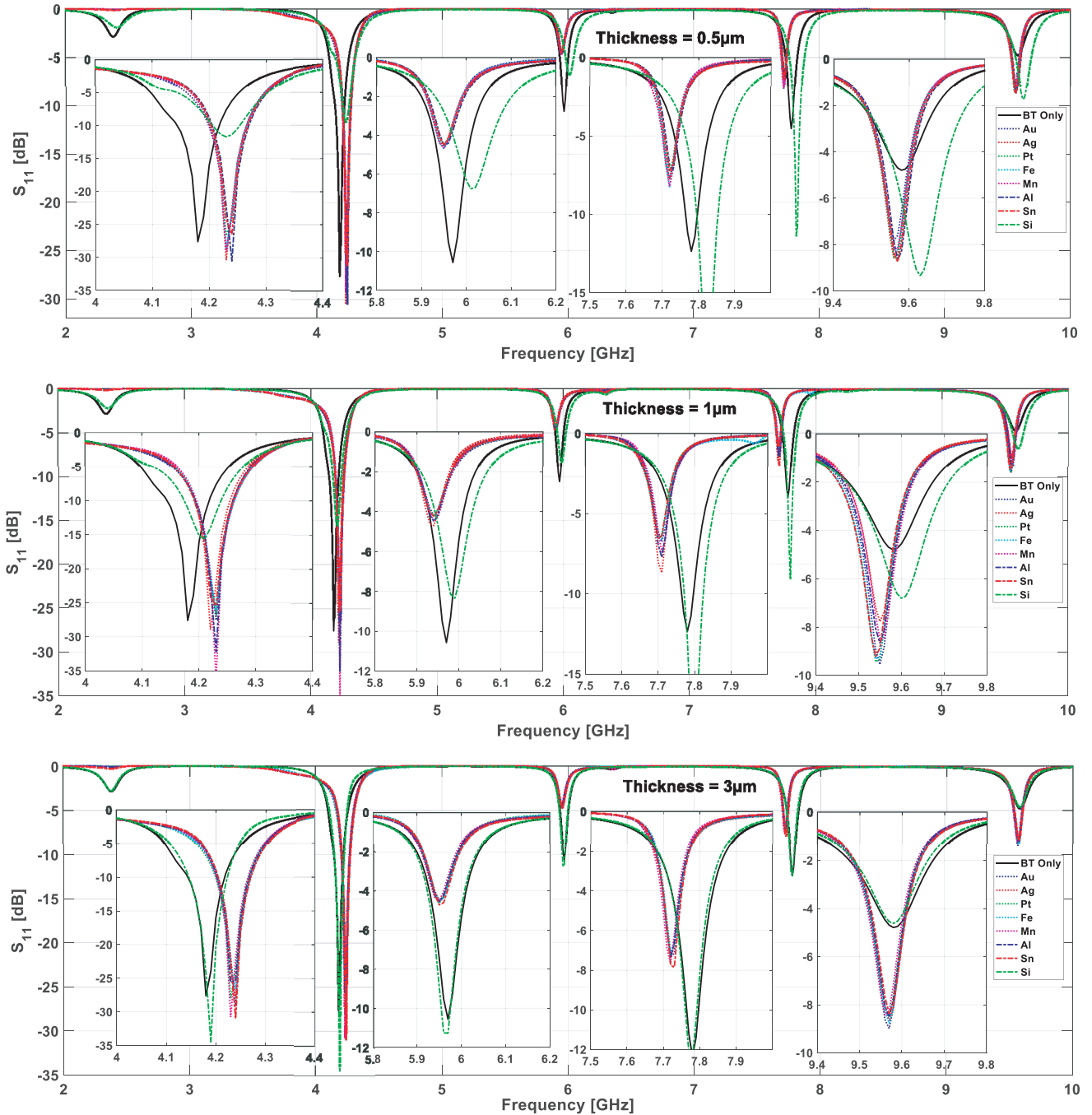
Figure 2. Bowtie S_{11} response testing with dielectric slabs of different permittivity values and thicknesses.

In this research, we have integrated our unique multi-band metamaterial, as a sensing enhancer, to create additional resonances, or points of detecting, in order to enhance metal detecting sensitivity. In the next section, we present our metamaterial (MTM) and its electromagnetic properties, followed by an MTM array integration with the bowtie to investigate the enhancement of metal detecting sensitivity.

Table 1. Electric conductivity [26, 30, 31].

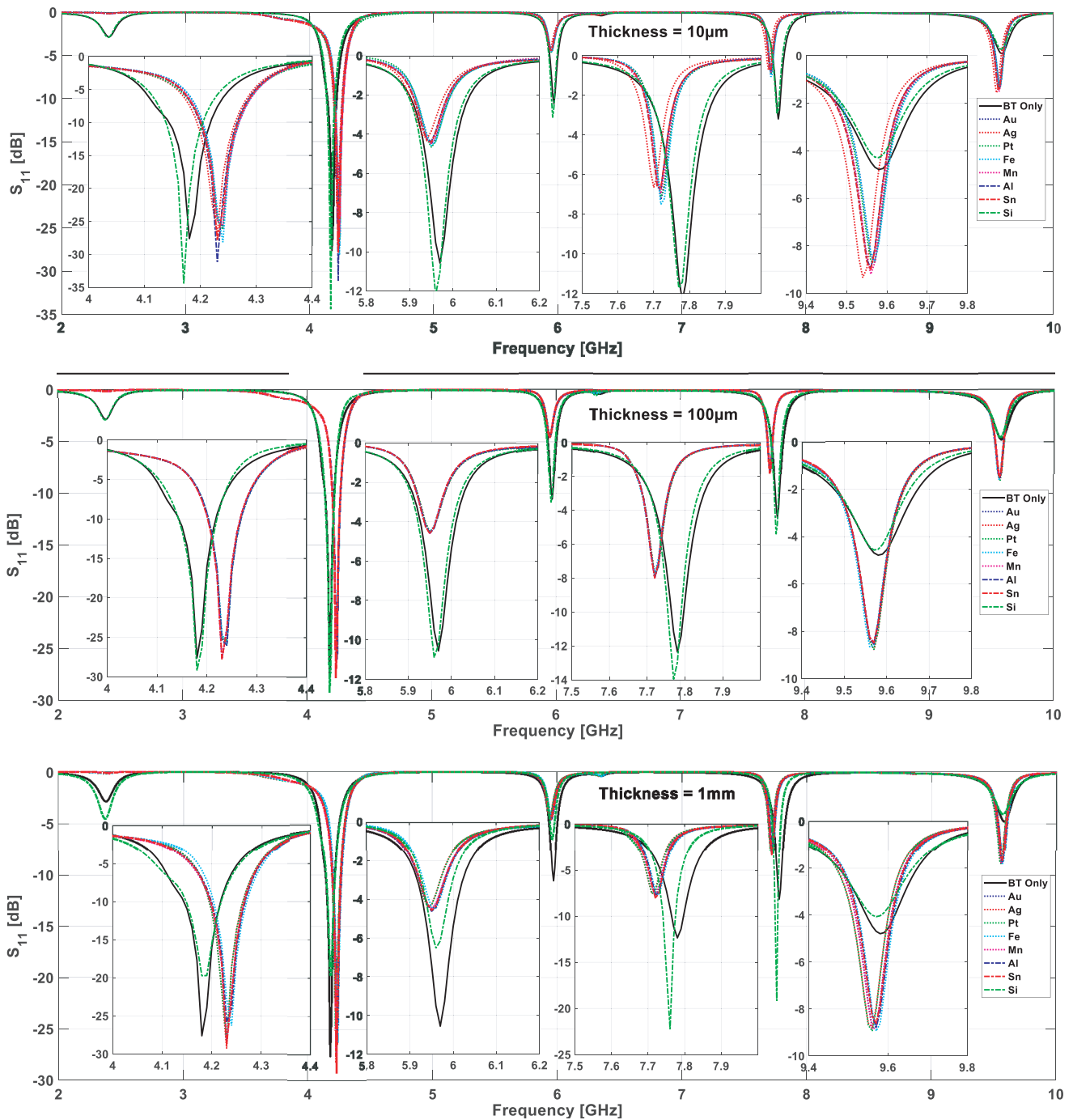|	Precious Transition Metal			Abundant Transition Metal		Post Transition or Basic Metal		Metalloid
	Ag	Pt	Au	Fe	Mn [28]	Al	Sn	Si
Electric Conductivity [S/m]	6.30e+7	9.43e+6	4.10e+7	1.04e+7	6.9e+5	3.56e+7	8.6957e+6	0.00025

Figure 3. Bowtie S_{11} response testing with thin metal and metalloid slabs of different thicknesses.

3. METAMATERIAL-INSPIRED SENSORS

3.1. Metamaterial Design

Metamaterials (MTMs), engineered or artificial electromagnetic materials, have been implemented in various electromagnetic applications, e.g., MTM-inspired sensors [20–25, 32–91] and MTM-inspired antennas [92–94]. Typical MTM structures are fabricated using metals or conductive materials, e.g., gold (Au), silver (Ag), palladium (Pd) [33, 42, 44, 45], and Copper (Cu) [38, 56]. Split ring resonators

(SRR) in both circular [23, 35, 50] and rectangular [32, 34, 36, 49, 55, 56] shapes, the most common MTM structures, are combined with a quarter wavelength transmission line or a simple antenna to design a compact electromagnetic contactless sensor. These SRR structures can be optimized as a separate [23, 48, 57, 59, 60] or concentric [35, 36, 49, 50, 55, 56] SRR array, derived from a conventional SRR. Other MTM shapes like H-shape [37, 51], X shape [43], omega shape [47], and U shape [45] are also found in some specific MTM-inspired sensors.

The broken symmetry or gap of a ring loop, excited by appropriate electric and magnetic-field orientations, creates electric and magnetic couplings, which generate a resonance. The inductance (L) and capacitance (C) formed by the material structure setting control the resonance location: $f = \sqrt{1/(L_T C_T)}$. By varying the MTM, transmission line and antenna dimensions, MTM-inspired sensors can be designed to operate work in the microwave regime or GHz range [23, 32, 34–36, 38, 41, 42, 46–48, 50, 52, 54–60] or up to a low optical regime in the tenth THz band [33, 37, 39, 40, 43–45, 49, 51, 53]. Multiple resonance bands can be easily manipulated by having MTM structure SRRs of different dimensions. MTM-inspired sensors then can be designed to operate in a single band [36, 37, 41–43, 46–49, 51] or multibands [23, 33, 34, 59–61] with higher sensitivity. MTM-inspired sensors have been employed for a variety of detecting purposes, for instance, liquidor fluid [23–25, 34, 43, 44, 46–48, 53–55, 57, 63, 65–69, 95], solid dielectric material [35, 36, 38, 52, 58, 62, 70], or biomaterials [37, 49, 50, 80, 91].

Quadruple homocentric circular SSRs with an aligned gap were initially designed to create four resonances; however, while the rings are slightly rotated, due to an extra broken symmetry, six additional resonances are created. Therefore, in this study, the misaligned gap four concentric SRRs, presented in Figure 4(a), have been implemented. The dimensions: $D1 = 31\,\text{mm}$, $D2 = 21\,\text{mm}$, $D3 = 15\,\text{mm}$,
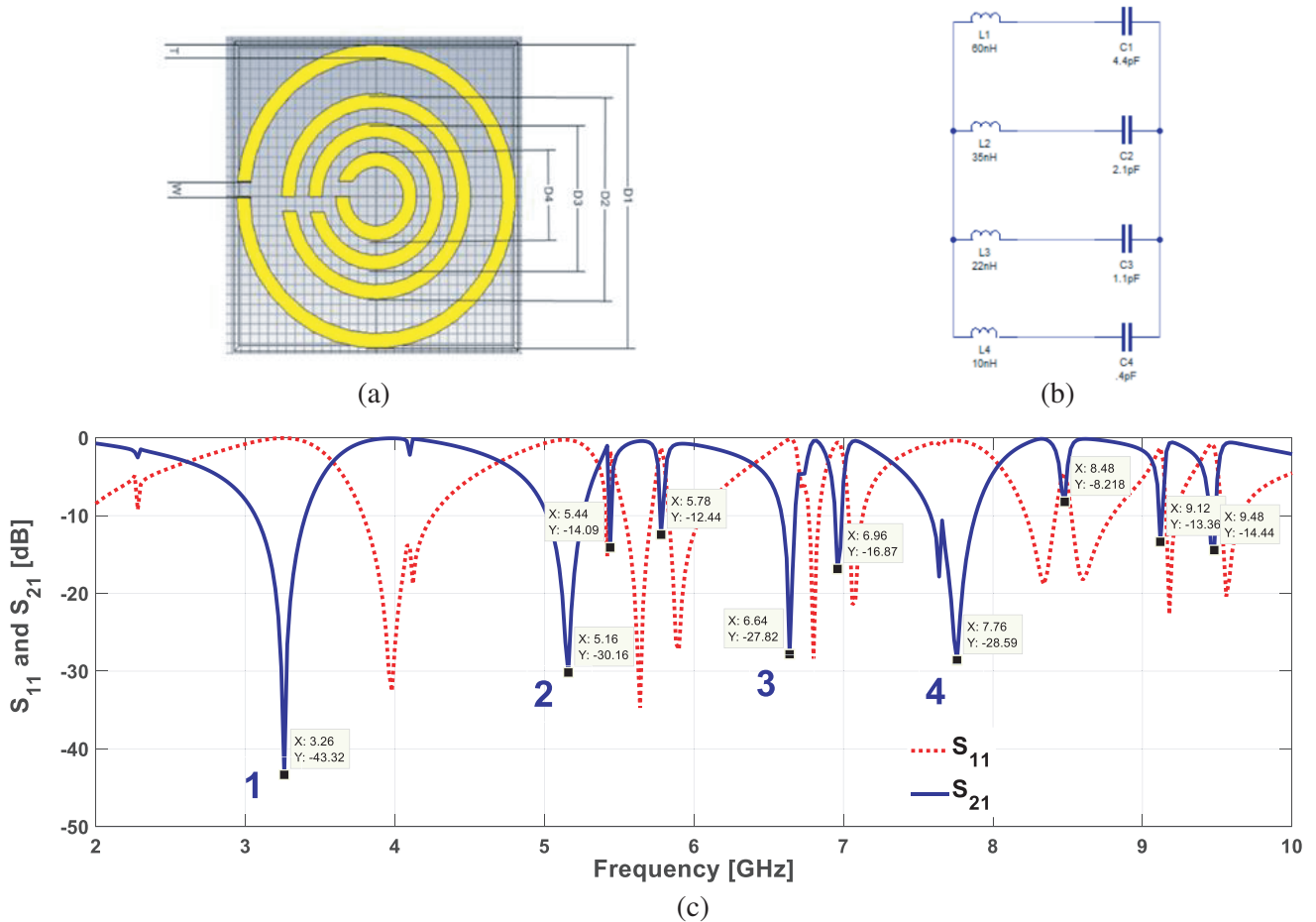

Figure 4. (a) Proposed quadruple concentric MTM structure, (b) its simplified equivalent circuit, and (c) S parameters.

$D4 = 9\,\text{mm}$, $W = 1.5\,\text{mm}$, and $T = 1.5\,\text{mm}$, were adjusted in order to manipulate the resonance locations within the C- and S-bands. An equivalent circuit of the MTM is shown in Figure 4(b). Each inductance (L) represents the line segments of the MTM structure, whilst the gaps are represented by capacitances (C). These inductances and capacitances were added in series and in parallel depending on their respective nodes. The inductance and capacitance were calculated using an approximation for the self-inductance of a circular loop and parallel plate capacitor formulas, respectively [96]. The MTM structures were built by a one-sided 1 oz Cu (0.03 mm thickness) 1.54 mm FR-4 ($\varepsilon_r = 4.4$) substrate. As projected, four major resonances, at 3.26 GHz, 5.16 GHz, 6.64 GHz, and 7.76 GHz, were generated. There were six additional minor resonances created within the S- and C-bands, i.e., 5.44 GHz, 5.78 GHz, 6.96 GHz, 8.48 GHz, 9.12 GHz, and 9.48 GHz. Figure 4(c) shows the transmission coefficient (S_{21}) and reflection coefficient (S_{11}) of the proposed quadruple concentric circular SRRs, where the ten resonances can be observed.

The results presented in the previous section have shown that the multi-band bowtie antenna can be used to classify dielectrics, metalloids, and metals; however, it is almost impossible to identify metals, even from different groups. We therefore were motivated to enhance the sensing and detecting property of the aforementioned bowtie by integrating the multi-band MTMs, and concentrated on precious metals, i.e., gold, silver, and platinum. These precious metals are transition metals located close together in the periodic table: VIIIB (Ru, Rh, Pd, Os, Ir, and Pt), and IB (Ag and Au) columns. Most precious metals share similar physical, thermal, and mechanical properties, while Ag and Au stand out for their low electrical resistivity and high thermal conductivity.

The proposed MTM array was inserted in between the bowtie antenna and the testing metal slab to create an MTM-inspired sensor, shown in Figure 5. The sensor sensitivity was optimized by varying the spacing between the bowtie antenna and the testing slab, h, (i.e., 3.75, 8.75, 13.75, 18.75, and 23.75 mm). The 18.75 mm showed the most pronounced detecting response, therefore was selected in this study. The distance, g, between the MTM array and the bowtie was fixed at 2.5 mm. The distance g, between the MTM array and the bowtie was fixed at 2.5 mm.
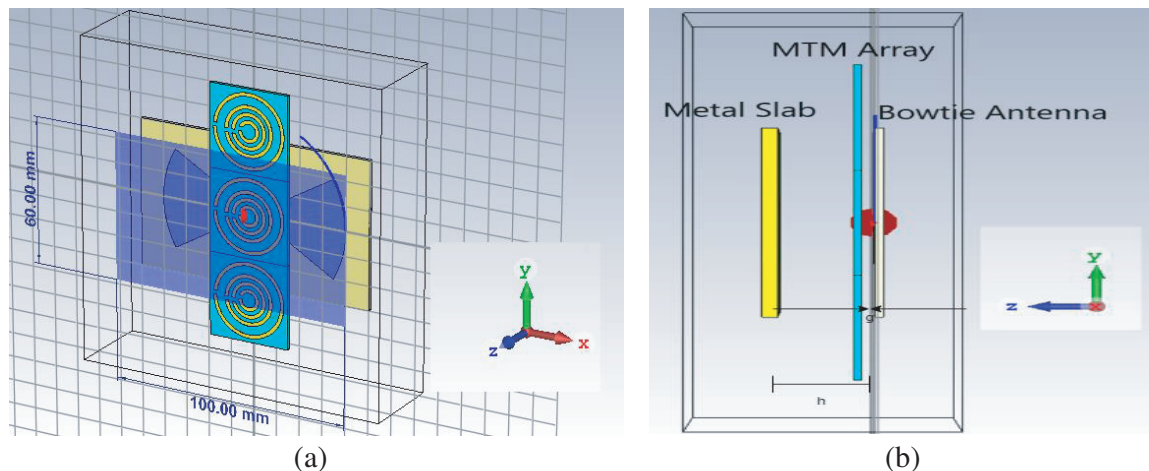

(a)　　　　　　　　　　　　　　(b)

Figure 5. Proposed MTM-inspired sensor.

3.2. MTM-Inspired Sensor Testing with Au, Ag, Pt Slabs of Various Thicknesses

The MTM-inspired sensor was tested with Au, Ag, and Pt slabs of various thicknesses: A1) 0.5, 0.6, and 0.7 μm; A2) 3, 5, 7, and 9 μm; A3) 0.1, 0.5, 1, and 2 mm. The comparison responses are presented in Figures 6–8.

A1) 0.5, 0.6, and 0.7 μm

Five resonances were found in between 2–8 GHz. Ag, Pt, and Au slabs with 0.5–0.7 μm thickness can be differentiated in the 4th resonance, 7.2–7.5 GHz.
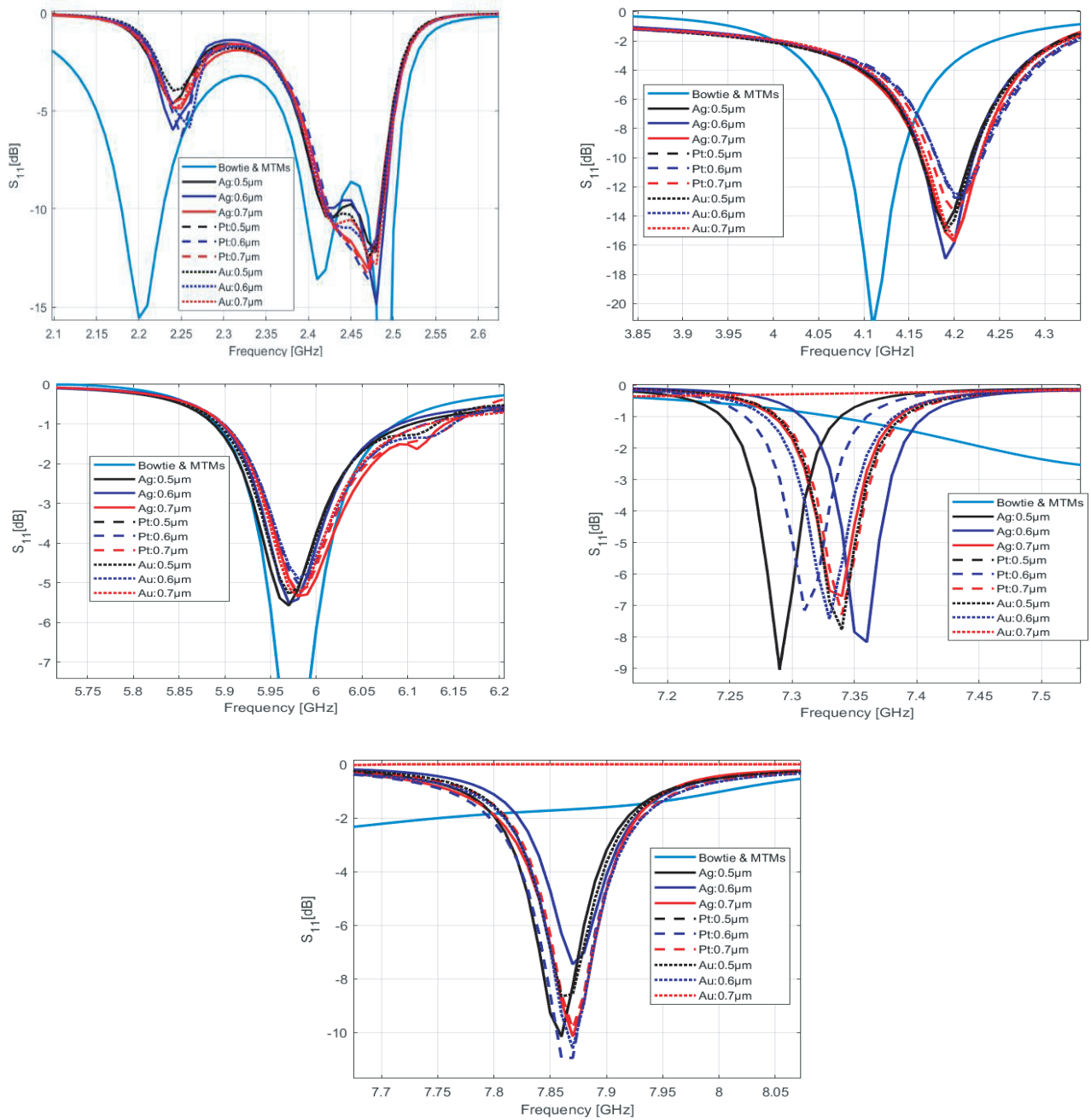
Figure 6. MTM-inspired sensor S_{11} response: Ag, Pt, Au slab of 0.5, 0.6 and 0.7 μm thickness.

A2) 3, 5, 7, and 9 μm

Five resonances were established in between 2–8 GHz, while the sensor was tested with Ag, Pt, and Au slabs of 3–9 μm thicknesses. Pt slabs were standing out at the 1st resonance, 2.1–2.6 GHz. Similar to slabs of 0.5–0.7 μm thicknesses, these Ag, Pt, and Au of 3–9 μm can be visibly separated in the 4th resonance, 7.2–7.5 GHz.
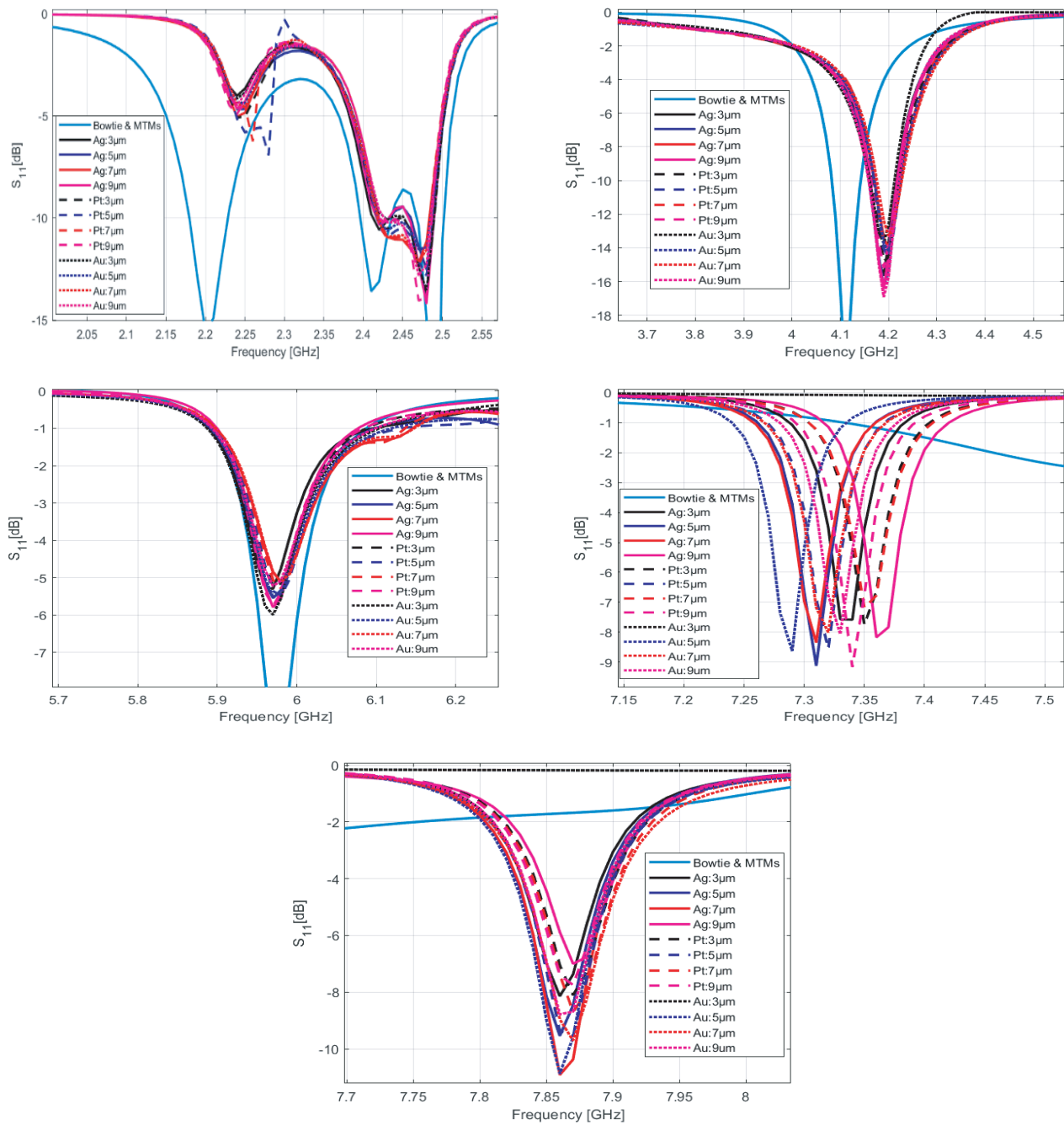
Figure 7. MTM-inspired sensor S_{11} response: Ag, Pt, Au slab of 3, 5, 7 and 9 μm thickness.

A3) 0.1, 0.5, 1, and 2 mm

Five resonances were also observed in the S- and C- bands, while the sensor was tested with Ag, Pt, and Au slabs of 0.1–2 mm thickness. The Ag, Pt, and Au slabs can be noticeably differentiated in the 4th resonance, 7.2–7.5 GHz, and also possibly distinguished in the other four resonances.
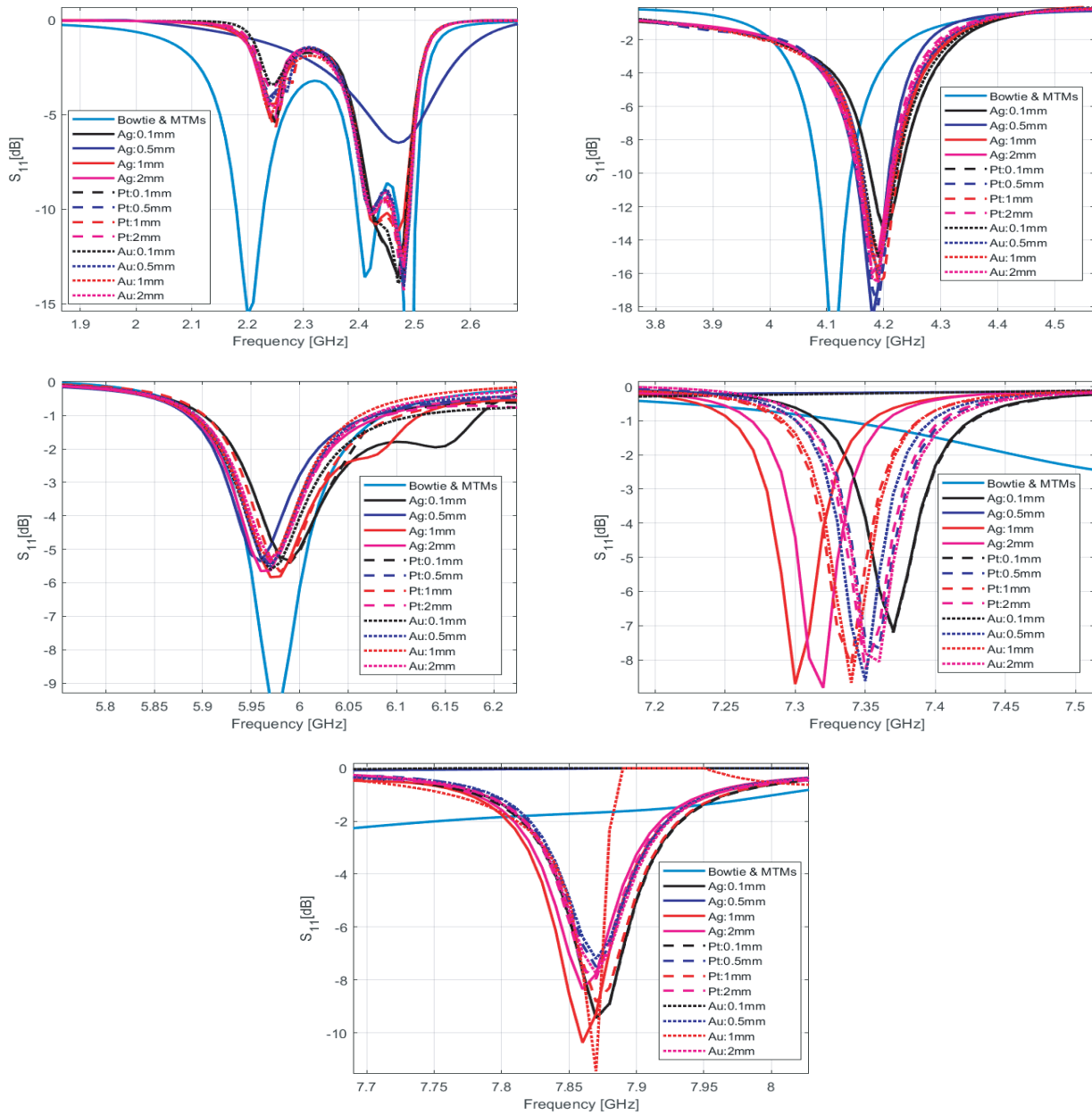
Figure 8. MTM-inspired sensor S_{11} response: Ag, Pt, Au slab of 0.1, 0.5, 1 and 2 mm thickness.

Next, the MTM-inspired sensor was tested with the Ag, Pt, and Au of various thicknesses, from 0.5 μm to 3 mm. The comparison responses are presented in Figures 9–14.

3.3. MTM-Inspired Sensor Testing with Ag Slabs

Five resonances were observed in the S- and C-bands, while the sensor was tested with Ag slabs of 0.5 μ–3 mm thicknesses. The Ag slabs of various thicknesses are noticeably differentiated in the 4th and 5th resonances, and are also possibly distinguished in the other three resonances.
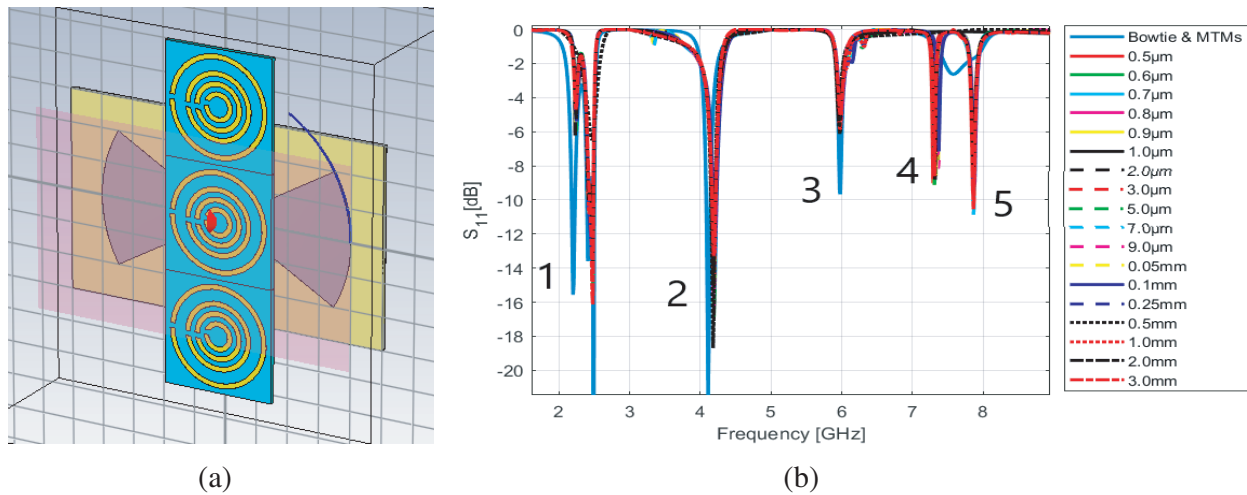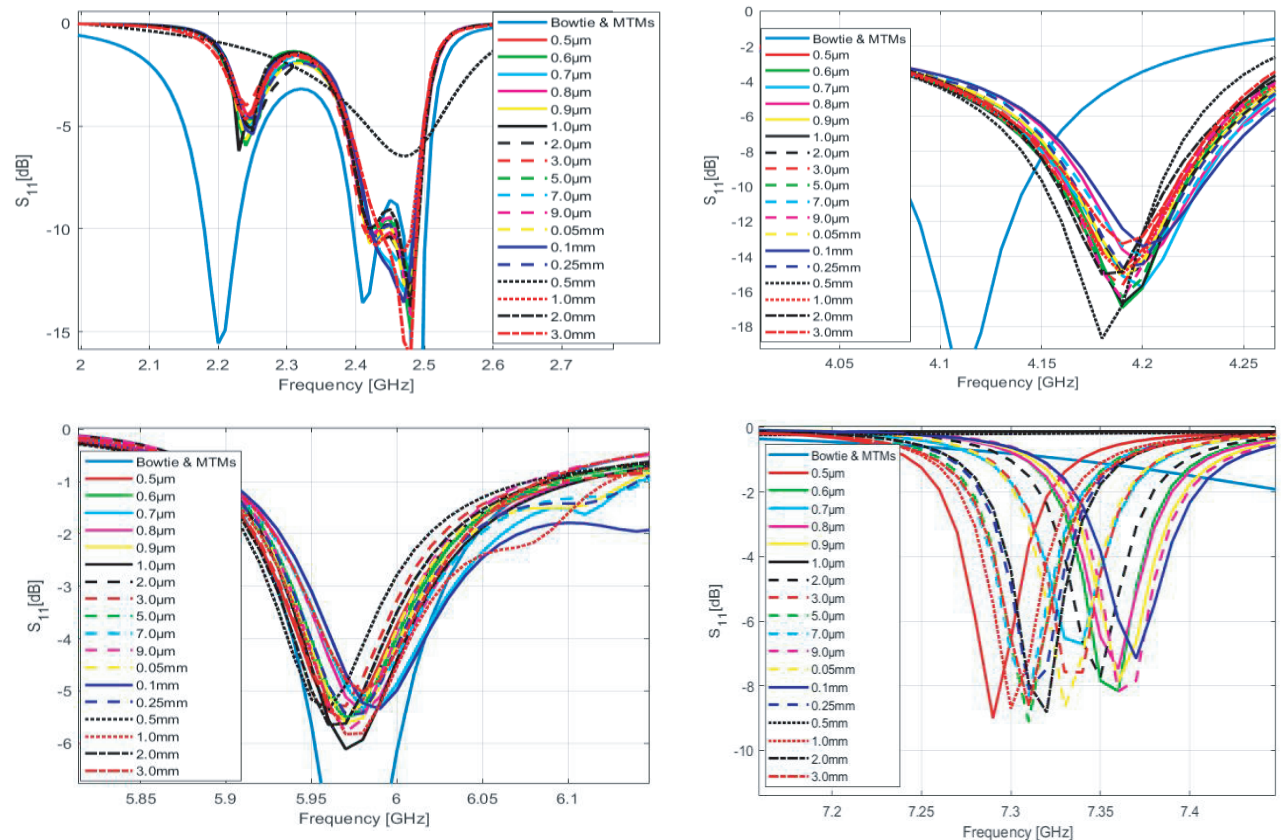

(a)   (b)

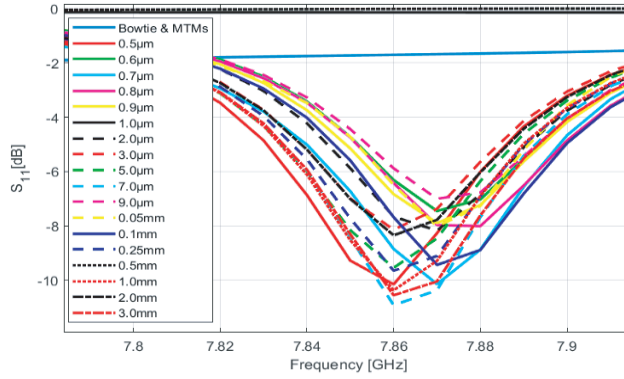**Figure 9.** (a) MTM-inspired bowtie sensor with Ag slab and (b) S_{11} results of various Ag thicknesses.

Figure 10. MTM-inspired sensor S_{11} response: Ag slab of $0.5\,\mu m$–$3\,mm$.

3.4. MTM-Inspired Sensor Testing with Pt Slabs

Five resonances were established in the observation band, while the sensor was tested with Pt slabs of $0.5\,\mu m$–$3\,mm$ thickness. The Pt slabs of different thicknesses are markedly differentiated in the 4th resonance and are also distinguished in the other four resonances.
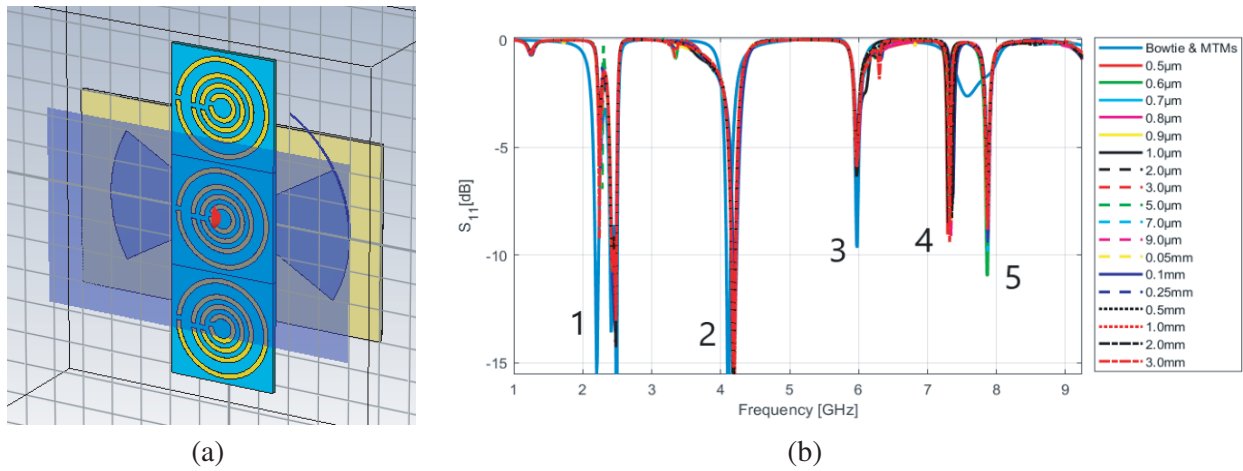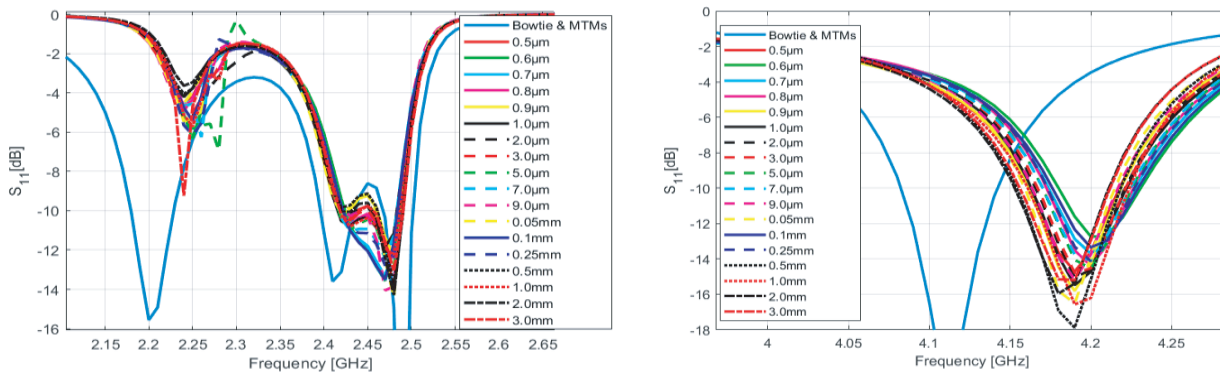

(a)   (b)

Figure 11. (a) MTM-inspired bowtie sensor with Pt slab and (b) S_{11} results of various Pt thicknesses.

Figure 12. MTM-inspired sensor S_{11} response: Pt slab of 0.5 μm–3 mm.

3.5. MTM-Inspired Sensor Testing with Au Slabs

Five resonances were found in the observation frequency band, while the sensor was tested with Au slabs of 0.5 μm–3 mm thicknesses. The Au slabs of different thicknesses are noticeably differentiated in the 4th resonance and are also possibly distinguished in the other four resonances.

(a)   (b)

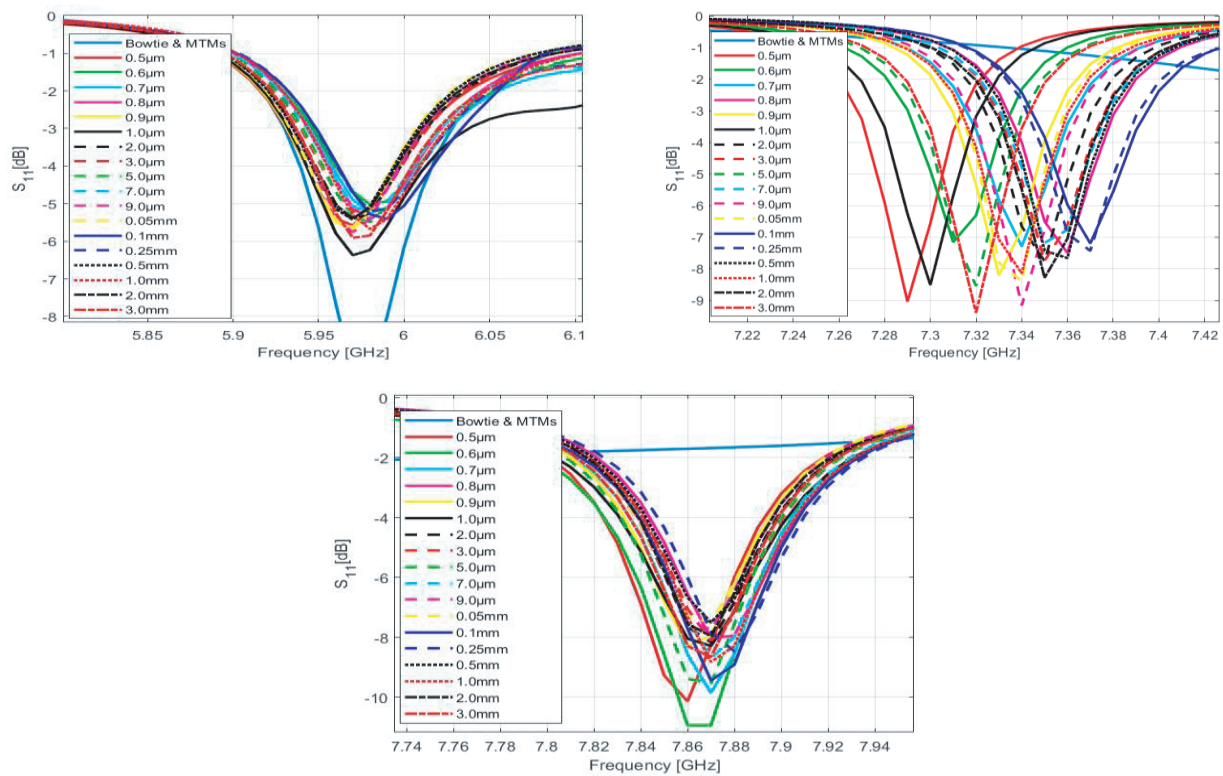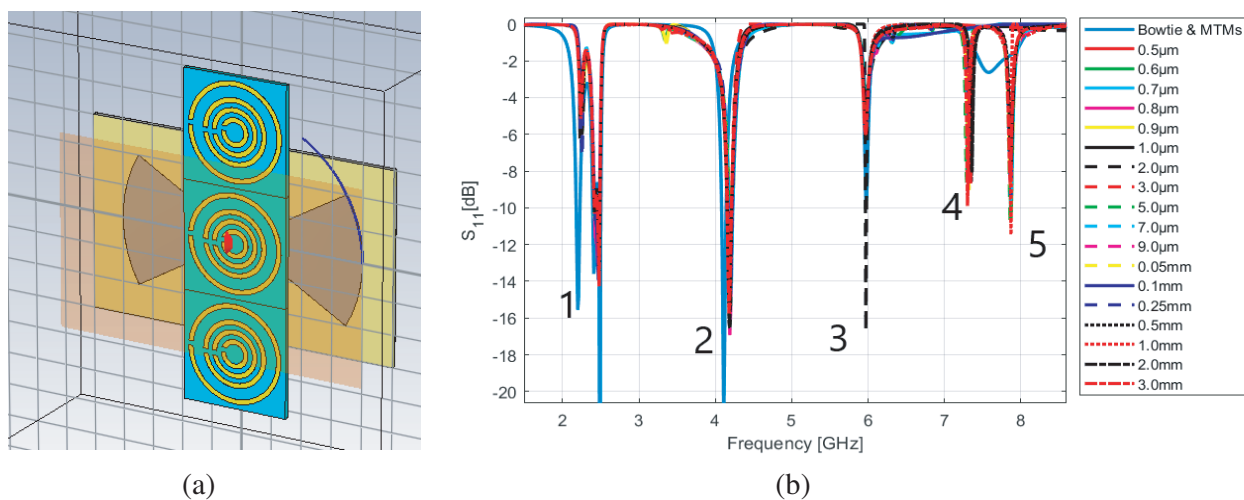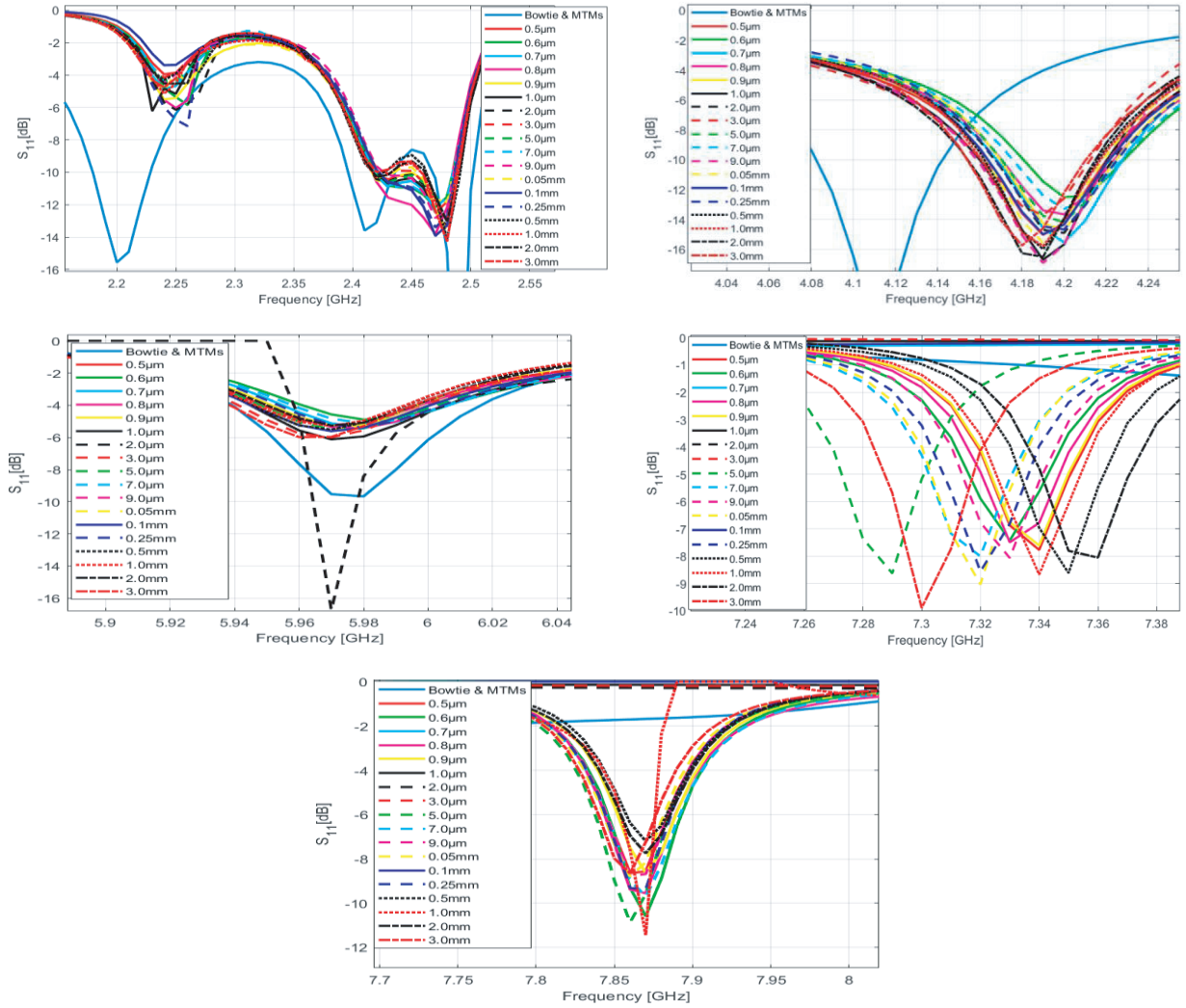**Figure 13.** (a) MTM-inspired bowtie sensor with Au slab and (b) S_{11} results of various Au thicknesses.

Figure 14. MTM-inspired sensor S_{11} response: Au slabs of 0.5 μm–3 mm.

4. CONCLUSION

A simple metamaterial-inspired sensor is proposed to discover and classify metals of different thicknesses in the microwave regime, within the S- and C-bands. The sensor is composed of an S- and C-band bowtie antenna and multi-band metamaterials. Five resonances of the reflection coefficients were established in the observation band, while the sensor was tested with three precious transition metal slabs, silver, platinum, and gold, of 0.5 μm–3 mm thicknesses. The metal slabs of different thicknesses are noticeably differentiated in the 4th resonance, in the 7.2–7.5 GHz range, and also possibly distinguished in the other four resonances. In order to improve the sensor's sensitivity, another antenna can be added as receiving port to collect the transmission coefficients, which can then be used to extract other electromagnetic parameters, for instance, complex permittivity and permeability, chirality, etc. These additional electromagnetic parameters can be used to further identify the metal contents.

ACKNOWLEDGMENT

REFERENCES

1. Gouyon, J., F. d'Orlyé, C. Simon, S. Griveau, C. Sella, L. Thouin, F. Bedioui, and A. Varenne, "Reversible microfluidics device for precious metal electrodeposition and depletion yield studies," *Electrochimica Acta*, Vol. 352, 136474, 2020, https://doi.org/10.1016/j.electacta.2020.136474.

2. Shahat, A. and S. Trupp, "Sensitive, selective, and rapid method for optical recognition of ultra-traces level of Hg(II), Ag(I), Au(III), and Pd(II) in electronic wastes," *Sensors and Actuators. B, Chemical*, Vol. 245, 789–802, 2017, https://doi.org/10.1016/j.snb.2017.02.008.

3. Mohamed, S., H. Hassan, A. Shahat, M. Awual, and R. Kamel, "A ligand-based conjugate solid sensor for colorimetric ultra-trace gold(III) detection in urban mining waste," *Colloids and Surfaces. A, Physicochemical and Engineering Aspects*, Vol. 581, 123842, 2019, https://doi.org/10.1016/j.colsurfa.2019.123842.

4. Elshehy, E., S. El-Safty, M. Shenashen, and M. Khairy, "Design and evaluation of optical mesocaptor for the detection/recovery of Au(III) from an urban mine," *Sensors and Actuators. B, Chemical*, Vol. 203, 363–374, 2014, https://doi.org/10.1016/j.snb.2014.06.055.

5. Elci, L., M. Soylak, and E. B. Buyuksekerci, "Separation of gold, palladium and platinum from metallurgical samples using an amberlite XAD-7 resin column prior to their atomic absorption spectrometric determinations," *Analytical Sciences*, Vol. 19, No. 12, 1621–1624, 2003, https://doi.org/10.2116/analsci.19.1621.

6. Yu, B., Y. Huang, J. Zhou, T. Guo, and B. Guan, "Real-time, in-situ analysis of silver ions using nucleic acid probes modified silica microfiber interferometry," *Talanta (Oxford)*, Vol. 165, 245–250, 2017, https://doi.org/10.1016/j.talanta.2016.12.053.

7. Santibáñez, M., R., Saavedra, J., Vedelago, F. Malano, and M. Valente, "Optimized EDXRF system for simultaneous detection of gold and silver nanoparticles in tumor phantom," *Radiation Physics and Chemistry (Oxford, England: 1993)*, Vol. 165, 108415, 2019, https://doi.org/10.1016/j.radphyschem.2019.108415.

8. Zhang, M., G. Zhu, T. Li, X. Lou, and L. Zhu, "A dual-channel optical fiber sensor based on surface plasmon resonance for heavy metal ions detection in contaminated water," *Optics Communications*, Vol. 462, 124750, 2020, https://doi.org/10.1016/j.optcom.2019.124750.

9. Funari, R., R. Ripa, B. Söderström, U. Skoglund, and A. Shen, "Detecting gold biomineralization by delftiaacidovorans biofilms on a quartz crystal microbalance," *ACS Sensors*, Vol. 4, No. 11, 3023–3033, 2019, https://doi.org/10.1021/acssensors.9b01580.

10. Zuber, A., M. Purdey, E. Schartner, C. Forbes, B. van der Hoek, D. Giles, A. Abell, T. Monro, and H. Ebendorff-Heidepriem, "Detection of gold nanoparticles with different sizes using absorption and fluorescence-based method," *Sensors and Actuators. B, Chemical*, Vol. 227, 117–127, 2016, https://doi.org/10.1016/j.snb.2015.12.044.

11. Ghosh, P. K., D. T. Debu, D. A. French, and J. B. Herzog, "Calculated thickness dependent plasmonic properties of gold nanobars in the visible to near-infrared light regime," *PloS One*, Vol. 12, No. 5, e0177463, 2017, https://doi.org/10.1371/journal.pone.0177463.

12. Li, S., H. Liu, L. Liu, Q. Lin, and X. Zhai, "Effect of silver film thickness on the surface plasma resonance in the rectangular Ag-Si-SiO$_2$ cavity," *Journal of Physics Communications*, Vol. 2, No. 5, 55024, 2018, https://doi.org/10.1088/2399-6528/aac52e.

13. Yamazaki, S., H. Nakane, and A. Tanaka, "Basic analysis of a metal detector," *IEEE Transactions on Instrumentation and Measurement*, Vol. 51, No. 4, 810–814, 2002, https://doi.org/10.1109/TIM.2002.803397.

14. Tang, Z. and L. J. Carter, "Metal detector head analysis," *2011 Fifth International Conference on Sensing Technology*, 93–96, 2011, https://doi.org/10.1109/ICSensT.2011.6137076.

15. Lahrech, A., A. Zaoui, F. Benyoubi, and A. Sakoub, "Modeling of inductive metal detector with swept frequency excitation," *2013 International Conference on Electromagnetics in Advanced Applications (ICEAA)*, 1305–1308, 2013, https://doi.org/10.1109/ICEAA.2013.6632461.

16. Liu, B. and W. Zhou, "The research of metal detectors using in food industry," *Proceedings of 2011 International Conference on Electronics and Optoelectronics*, Vol. 4, V4-43–V4-45, 2011, https://doi.org/10.1109/ICEOE.2011.6013421.

17. Bedenik, G., J. Silveira, I. Santos, E. Carvalho, J. Carvalho, and R. Freire, "Single coil metal detector and classifier based on phase measurement," *2019 4th International Symposium on Instrumentation Systems, Circuits and Transducers (INSCIT)*, 1–6, 2019, https://doi.org/10.1109/INSCIT.2019.8868329.

18. Sharawi, M. and M. Sharawi, "Design and implementation of a low-cost VLF metal detector with metal-type discrimination capabilities," *2007 IEEE International Conference on Signal Processing and Communications*, 480–483, 2007, https://doi.org/10.1109/ICSPC.2007.4728360.

19. Zhang, N., J. Cao, S. Wang, S. Wang, and S. Wang, "Design and calculation of planar eddy current coil in coin identification," *IEEE Transactions on Applied Superconductivity*, Vol. 26, No. 7, 1–4, 2016, https://doi.org/10.1109/TASC.2016.2594860.

20. Su, L., J. Naqui, J. Mata-Contreras, and F. Martin, "Modeling metamaterial transmission lines loaded with pairs of coupled split-ring resonators," *IEEE Antennas and Wireless Propagation Letters*, Vol. 14, 68–71, 2015, https://doi.org/10.1109/LAWP.2014.2355035.

21. Wongkasem, N. and M. Ruiz, "Multi-negative index band metamaterials-inspired microfluidic sensors," *Progress In Electromagnetic Research C*, Vol. 94, 29–44, 2019.

22. Ruiz, M. and N. Wongkasem, "Development of X-band metamaterial-inspired sensors for dielectric constant detection," *IEEE AP-S Conference Proceedings*, 1–2, Atlanta, USA, July 2019.

23. Zhou, H., D. Hu, C. Yang, C. Chen, J. Ji, M. Chen, Y. Chen, Y. Yang, and X. Mu, "Multi-band sensing for dielectric property of chemicals using metamaterial integrated microfluidic sensor," *Scientific Reports*, Vol. 8, No. 1, 1–al, 2018l, https://doi.org/10.1038/s41598-018-32827-y.

24. Salim, A. and S. Lim, "Review of recent metamaterial microfluidic sensors," *Sensors (Basel, Switzerland)*, Vol. 18, No. 1, 232, 2018, https://doi.org/10.3390/s18010232.

25. Liu, W., H. Sun, and L. Xu, "A microwave method for dielectric characterization measurement of small liquids using a metamaterial-based sensor," *Sensors (Basel, Switzerland)*, Vol. 18, No. 5, 1438, 2018, https://doi.org/10.3390/s18051438.

26. CST Microwave Studio Suites, https://www.3ds.com/products-services/simulia/products/cst-studio-suite/CST, accessed on January 1, 2021.

27. Helmenstine, A. M., "Transition metals: List and properties," thoughtco.com/transition-metals-list-and-properties-606663, ThoughtCo, August 28, 2020.

28. "Wikipedia: Post-transition metal," available: https://ipfs.io/ipfs/QmXoypizjW3WknFiJnKLwH-CnL72vedxjQkDDP1mXWo6uco/wiki/Post-transition_metal.html, last modified January 31, 2021.

29. Flowers, P., K. Theopold, R. Langley, and W. R. Robinson, *Chemistry 2e*, 2nd Edition, Openstax, XanEdu Publishing Inc, 2019.

30. Weast, R. C., *CRC Handbook of Chemistry and Physics*, CRC Press, Boca Raton, Florida, 1988.

31. "Wikipedia: Manganese," available: https://en.wikipedia.org/wiki/Manganese, last modified January 31, 2021.

32. Memon, M., A. Salim, H. Jeong, and S. Lim, "Metamaterial inspired radio frequency-based touchpad sensor system," *IEEE Transactions on Instrumentation and Measurement*, Vol. 69, No. 4, 1344–1352, 2020, https://doi.org/10.1109/TIM.2019.2908507.

33. Chamoli, S., S. Singh, and C. Guo, "Metal-Dielectric-Metal metamaterial-based hydrogen sensors in the water transmission window," *IEEE Sensors Letters*, Vol. 4, No. 5, 1–4, 2020, https://doi.org/10.1109/LSENS.2020.2991081.

34. Zahertar, S., E. Laurin, L. Dodd, and H. Torun, "Embroidered rectangular split-ring resonators for the characterization of dielectric materials," *IEEE Sensors Journal*, Vol. 20, No. 5, 2434–2439, 2020, https://doi.org/10.1109/JSEN.2019.2953251.

35. Shahzad, W., W. Hu, A. Samad, and L. Ligthart, "Complementary split ring resonator based metamaterial sensor for dielectric materials measurements," *2020 17th International Bhurban Conference on Applied Sciences and Technology (IBCAST)*, 695–698, 2020, https://doi.org/10.1109/IBCAST47879.2020.9044550.

36. Samad, A., W. Hu, W. Shahzad, and L. Ligthart, "Design and simulation of metamaterial sensor and numerical formulation for dielectric properties," *2020 17th International Bhurban Conference on Applied Sciences and Technology (IBCAST)*, 714–716, 2020, https://doi.org/10.1109/IBCAST47879.2020.9044571.

37. Li, D., S. Lin, F. Hu, Z. Chen, W. Zhang, and J. Han, "Metamaterial terahertz sensor for measuring thermal-induced denaturation temperature of insulin," *IEEE Sensors Journal*, Vol. 20, No. 4, 1821–1828, 2020, https://doi.org/10.1109/JSEN.2019.2949617.

38. Samad, A., W. Hu, W. Shahzad, and H. Raza, "Design of DS-CSRR based microwave sensor for efficient measurement of dielectric constant of materials," *2020 5th International Conference on Computer and Communication Systems (ICCCS)*, 821–824, 2020, https://doi.org/10.1109/ICCCS49078.2020.9118544.

39. Saadeldin, A., M. Hameed, E. Elkaramany, and S. Obayya, "Highly sensitive terahertz metamaterial sensor," *IEEE Sensors Journal*, Vol. 19, No. 18, 7993–7999, 2019, https://doi.org/10.1109/JSEN.2019.2918214.

40. Ma, L., Z. Cui, D. Zhu, L. Yue, L. Hou, and Y. Wang, "Metamaterials sensor based on multiband terahertz absorber," *2019 44th International Conference on Infrared, Millimeter, and Terahertz Waves (IRMMW-THz)*, 1–2, 2019, https://doi.org/10.1109/IRMMW-THz.2019.8874505.

41. Yudistira, H. T. and M. Asril, "Preliminary study of microwave metamaterial based on cylinder-shaped for sensor," *2019 6th International Conference on Instrumentation, Control, and Automation (ICA)*, 203–206, 2019, https://doi.org/10.1109/ica.2019.8916692.

42. Govind, G. and M. Akhtar, "Metamaterial-inspired microwave microfluidic sensor for glucose monitoring in aqueous solutions," *IEEE Sensors Journal*, Vol. 19, No. 24, 11900–11907, 2019, https://doi.org/10.1109/JSEN.2019.2938853.

43. Huang, S., Y. Hu, S. Hsu, K. Tang, T. Yen, and D. Yao, "X-shaped metamaterial biosensor combined with microfluidic system for different IPA concentration measurement," *2019 44th International Conference on Infrared, Millimeter, and Terahertz Waves (IRMMW-THz)*, 1–2, 2019, https://doi.org/10.1109/IRMMW-THz.2019.8873860.

44. Wu, Y., Y. Meng, B. Yakupoglu, and M. Adams, "A metamaterial/liquid-core waveguide microfluidic optical sensor," *Sensors and Actuators. A, Physical*, Vol. 300, 111592, 2019, https://doi.org/10.1016/j.sna.2019.111592.

45. Agarwal, S. and Y. Prajapati, "Metamaterial based sucrose detection sensor using transmission spectroscopy," *Optik (Stuttgart)*, Vol. 205, 164276, 2020, https://doi.org/10.1016/j.ijleo.2020.164276.

46. Caetano da Silva, J. and V. Rodriguez-Esquerre, "Metamaterial waveguides as integrated optics sensor," *Optik (Stuttgart)*, Vol. 212, 164756, 2020, https://doi.org/10.1016/j.ijleo.2020.164756.

47. Altıntaş, O., M. Aksoy, and E. Ünal, "Design of a metamaterial-inspired omega shaped resonator-based sensor for industrial implementations," *Physica. E, Low-Dimensional Systems & Nanostructures*, Vol. 116, 113734, 2020, https://doi.org/10.1016/j.physe.2019.113734.

48. Gulsu, M., F. Bagci, S. Can, A. Yilmaz, and B. Akaoglu, "Metamaterial-based sensor with a polycarbonate substrate for sensing the permittivity of alcoholic liquids in a WR-229 waveguide," *Sensors and Actuators. A, Physical*, Vol. 312, 112139, 2020, https://doi.org/10.1016/j.sna.2020.112139.

49. Tang, M., L. Xia, D. Wei, S. Yan, M. Zhang, Z. Yang, H. Wang, C. Du, and H. Cui, "Rapid and label-free metamaterial-based biosensor for fatty acid detection with terahertz time-domain spectroscopy," *Spectrochimica Acta. Part A, Molecular and Biomolecular Spectroscopy*, Vol. 228, 117736, 2020, https://doi.org/10.1016/j.saa.2019.117736.

50. Hossain, T., M. Jamlos, M. Jamlos, F. Dzaharudin, M. Ismail, S. Al-Bawri, S. Sugumaran, and M. Ahmad Salimi, "Bandwidth enhancement of five-port reflectometer-based ENG DSRR metamaterial for microwave imaging application," *Sensors and Actuators. A, Physical*, Vol. 303, 111638, 2020, https://doi.org/10.1016/j.sna.2019.111638.

51. Faruk, A. and C. Sabah, "Absorber and sensor applications of complimentary H-shaped fishnet metamaterial for sub-terahertz frequency region," *Optik (Stuttgart)*, Vol. 177, 64–70, 2019, https://doi.org/10.1016/j.ijleo.2018.09.145.

52. Yelizarov, A., A. Kukharenko, and A. Skuridin, "Metamaterial-based sensor for measurements of physical quantities and parameters of technological processes," *2018 12th International Congress on Artificial Materials for Novel Wave Phenomena (Metamaterials)*, 448–450, 2018, https://doi.org/10.1109/MetaMaterials.2018.8534122.

53. Luo, J., R. Xu, W. Chen, J. Sha, K. Yan, D. Yao, X. Liu, S. Liao, J. Zhong, S. Yang, Y. Yu, Y. Tong, Z. Xu, and Y. Lin, "An ultra-sensitive glucose sensor by using metamaterial-based microfluidic chip," *2018 International Conference on Optical MEMS and Nanophotonics (OMN)*, 1–2, 2018, https://doi.org/10.1109/OMN.2018.8454547.

54. Zhou, Y., J. Cai, L. Yang, and C. Zhang, "Highly sensitive microwave microfluidic chemical sensors based on metamaterials," *2018 IEEE International Conference on Computational Electromagnetics (ICCEM)*, 1–3, 2018, https://doi.org/10.1109/COMPEM.2018.8496587.

55. Chuma, E., Y. Iano, G. Fontgalland, and L. Bravo Roger, "Microwave sensor for liquid dielectric characterization based on metamaterial complementary split ring resonator," *IEEE Sensors Journal*, Vol. 18, No. 24, December 15, 2018.

56. Shaw, T. and D. Mitra, "Electromagnetic metamaterial-based sensor design for chemical discrimination," *2017 IEEE MTT-S International Microwave and RF Conference (IMaRC)*, 271–274, 2017.

57. Velez, P., L. Su, K. Grenier, J. Mata-Contreras, D. Dubuc, and F. Martin, "Microwave microfluidic sensor based on a microstrip splitter/combiner configuration and Split Ring Resonators (SRRs) for dielectric characterization of liquids," *IEEE Sensors Journal*, Vol. 17, No. 20, October 15, 2017.

58. Shi, P., R. Gao, S. Liu, and Y. Yuan, "Topology optimization-based design of metamaterial-inspired sensor with improved sensitivity," *Sensors and Actuators. A, Physical*, Vol. 268, 83–90, 2017, https://doi.org/10.1016/j.sna.2017.10.050.

59. Sekkache, H. and M. Lashab, "Study and design of a sensor containing metamaterials, application into biomedical," *2018 International Conference on Advanced Systems and Electric Technologies (IC_ASET)*, 2018.

60. Withayachumnankul, W., K. Jaruwongrungsee, C. Fumeaux, and D. Abbott, "Metamaterial-inspired multichannel thin-film sensor," *IEEE Sensors Journal*, Vol. 12, No. 5, May 2012.

61. Bakır, M., M. Karaaslan, E. Unal, F. Karadag, F. O. Alkurt, O. Altıntaş, S. Dalgac, and C. Sabah, "Microfluidic and fuel adulteration sensing by using chiral metamaterial sensor," *J. Electrochem. Soc.*, Vol. 165, 11, 2018.

62. Su, L., J. Mata-Contreras, P. Velez, and F. Martin, "A review of sensing strategies for microwave sensors based on metamaterial-inspired resonator: Dielectric characterization, displacement, and angular velocity measurements for health diagnosis, telecommunication, and space applications," *Int. J. of Antennas and Propagation*, 5619728, 2017.

63. Bakir, M., "Electromagnetic-based microfluidic sensor applications," *J. Electrochem. Soc.*, Vol. 164, B488–B494, 2017.

64. Shih, K., P. Pitchappa, M. Manjappa, C. P. Ho, R. Singh, and C. Lee, "Microfluidic metamaterial sensor: Selective trapping and remote sensing of microparticles," *J. Appl. Phys.*, Vol. 121, 023102, 2017.

65. Saghati, A. P., J. S. Batra, J. Kameoka, and K. Entesari, "A metamaterial-inspired wideband microwave interferometry sensor for dielectric spectroscopy of liquid chemicals," *IEEE Trans. Microw. Theory Tech.*, Vol. 65, 2558–2570, 2017.

66. Sadeqi, A. and S. Sonkusale, "Low-cost metamaterial-on-paper chemical sensor," *Transducers Int. Conf. Solid-State Sens., Actuators Microsyst.*, Vol. 25, 1437–1440, 2017.

67. Awang, R. A., F. J. Tovar-Lopez, T. Baum, S. Sriram, and W. S. T. Rowe, "Meta-atom microfluidic sensor for measurement of dielectric properties of liquids," *J. Appl. Phys.*, Vol. 121, 094506, 2017.

68. Salim, A. and S. Lim, "Complementary split-ring resonator-loaded microfluidic ethanol chemical sensor," *Sensors*, Vol. 16, 1802, 2016.

69. Kim, H. K., D. Lee, and S. A. Lim, "Fluidically tunable metasurface absorber for fexible large-scale wireless ethanol sensor applications," *Sensors*, Vol. 16, 1246, 2016.

70. Long, J. and B. Wang, "A metamaterial-inspired sensor for combined inductive-capacitive," *Appl. Phys. Lett.*, Vol. 106, 074104, 2015.

71. Kim, H. K., M. Yoo, and S. Lim, "Novel ethanol chemical sensor using microfluidic metamaterial," *Proceedings of the IEEE International Symposium on Antennas and Propagation & National Radio Science Meeting*, 1358–1359, Vancouver, BC, Canada, July 2015.

72. Byford, J. A., K. Y. Park, and P. Chahal, "Metamaterial inspired periodic structure used for microfluidic sensing," *Proceedings of the Electronic Components Technology Conference*, 1997–2002, San Diego, CA, USA, May 2015.

73. Rawat, V., S. Dhobale, and S. N. Kale, "Ultra-fast selective sensing of ethanol and petrol using microwave-range metamaterial complementary split-ring resonators," *J. Appl. Phys.*, Vol. 116, 164106, 2014.

74. Ebrahimi, A., W. Withayachumnankul, S. Al-Sarawi, and D. Abbott, "High-sensitivity metamaterial-inspired sensor for microfluidic dielectric characterization," *IEEE Sensors Journal*, Vol. 14, No. 5, 2014.

75. Abduljabar, A., D. J. Rowe, A. Porch, and D. A. Barrow, "Novel microwave microfluidic sensor using a microstrip split-ring resonator," *IEEE Trans. Microw. Theory Tech.*, Vol. 62, 679–688, 2014.

76. Withayachumnankul, W., K. Jaruwongrungsee, A. Tuantranont, C. Fumeaux, and D. Abbott, "Metamaterial-based microfluidic sensor for dielectric characterization," *Sensors and Actuators. A, Physical*, Vol. 189, 233–237, 2013.

77. Chretiennot, T., D. Dubuc, and K. Grenier, "A microwave and microfluidic planar resonator for efficient and accurate complex permittivity characterization of aqueous solutions," *IEEE Trans. Microw. Theory Techn.*, Vol. 61, No. 2, 972–978, 2013.

78. Agarwal, S. and Y. K. Prajapati, "Multifunctional metamaterial surface for absorbing and sensing applications," *Optics Communications*, Vol. 439, No. 15, 304–307, 2019.

79. Agarwal, S., Y. K. Prajapati, and V. Mishra, "Thinned fibrebragg grating as a fuel adulteration sensor: Simulation and experimental study," *Opto-Electronics Review*, Vol. 23, No. 4, 231–238, 2015.

80. Afapour, Z. O. V., Y. A. H. Ajati, and M. O. H. Ajati, "Graphene-based mid-infrared biosensor," *J. Opt. Soc. Am. B*, Vol. 34, 2586–2592, 2017.

81. Geng, Z., X. Zhang, Z. Fan, X. Lv, and H. Chen, "A route to terahertz metamaterial biosensor integrated with microfluidics for liver cancer biomarker testing in early stage," *Sci. Rep.*, Vol. 7, 1–11, 2017.

82. Sreekanth, K. V., Y. Alapan, M. El Kabbash, E. Ilker, M. Hinczewski, U. A. Gurkan, A. De Luca, and G. Strangi, "Extreme sensitivity biosensing platform based on hyperbolic metamaterials," *Nat. Mater.*, Vol. 15, 621–627, 2016.

83. Aristov, A. I., M. Manousidaki, A. Danilov, K. Terzaki, C. Fotakis, M. Farsari, and A. V. Kabashin, "3D plasmonic crystal metamaterials for ultra-sensitive biosensing," *Sci. Rep.*, Vol. 6, 1–8, 2016.

84. Chen, M., F. Fan, S. Shen, X. Wang, and S. Chang, "Terahertz ultrathin film thickness sensor below $\lambda/90$ based on metamaterial," *Appl. Opt.*, Vol. 55, 6471–6474, 2016.

85. Lee, D.-K. K., J.-H. H. Kang, J.-S. S. Lee, H.-S. S. Kim, C. Kim, J. Hun Kim, T. Lee, J.-H. H. Son, Q.-H. H. Park, and M. Seo, "Highly sensitive and selective sugar detection by terahertz nano-antennas," *Sci. Rep.*, Vol. 5, 1–7, 2015.

86. Wu, P. C., G. Sun, W. T. Chen, K. Y. Yang, Y. W. Huang, Y. H. Chen, H. L. Huang, W. L. Hsu, H. P. Chiang, and D. P. Tsai, "Vertical split-ring resonator based nanoplasmonic sensor," *Appl. Phys. Lett.*, Vol. 105, 3898, 2014.

87. Torun, H., F. Cagri Top, G. Dundar, and A. D. Yalcinkaya, "An antenna-coupled split-ring resonator for biosensing," *J. Appl. Phys.*, Vol. 116, 124701, 2014.

88. Lee, H. J., J. H. Lee, H. S. Moon, I. S. Jang, J. S. Choi, J. G. Yook, and H. Jung, "A planar splitring resonator-based microwave biosensor for label-free detection of biomolecules," *Sens. Actuators B Chem.*, Vol. 169, 26–31, 2012.

89. Chen, T., S. Li, and H. Sun, "Metamaterials application in sensing," *Sensors*, Vol. 12, 2742–2765, 2012.

90. Zijlstra, P., P. M. R. Paulo, and M. Orrit, "Optical detection of single non-absorbing molecules using the surface plasmon resonance of a gold nanorod," *Nat. Nanotechnol.*, Vol. 7, 379–382, 2012.

91. Lee, H. J. and J. G. Yook, "Biosensing using split-ring resonators at microwave regime," *Appl. Phys. Lett.*, Vol. 92, 10–13, 2008.

92. Thankachan, S. and B. Paul, "A compact metamaterial inspired CPW fed multiband monopole antenna for wireless applications," *2020 IEEE International Symposium on Antennas and Propagation and North American Radio Science Meeting,* 427–428, 2020, https://doi.org/10.1109/IEEECONF35879.2020.9329799.

93. Christydass, S. and N. Gunavathi, "Co-directional CSRR inspired printed antenna for locomotive short range radar," *2017 International Conference on Inventive Computing and Informatics (ICICI)*, 627–630, 2017, https://doi.org/10.1109/ICICI.2017.8365209.

94. Mishra, A., M. Ameen, and R. Chaudhary, "A compact triple band metamaterial inspired antenna using SRR and hexagonal stub for UMTS, WLAN, and WiMAX applications in S/C bands," *2019 URSI Asia-Pacific Radio Science Conference (AP-RASC)*, 1–4, 2019, https://doi.org/10.23919/URSIAP-RASC.2019.8738481.

95. White, G. M., "The origins and the future of microfluidics," *Nature*, Vol. 442, 368–373, 2006.

96. Arritt, B. J., D. R. Smith, and T. Khraishi, "Equivalent circuit analysis of metamaterial strain dependent effective medium parameters," *J. of Applied Science*, Vol. 109, 073512, 2011.